

## Supplementary Material

### Effects of Metal Film Thickness and Gain on the Coupling of Organic Semiconductor Emission to Surface Plasmon Polaritons

Ankur K. Dalsania, Jesse Kohl, Cindy E. Kumah, Zeqing Shen, Christopher E. Petoukhoff, Catrice M. Carter, Deirdre M. O'Carroll\*

#### S1. Supplementary ISMI Waveguide Characterization

##### S1.1 Transmittance Measurements

In order to calculate absorbance at 355 nm for the samples, the transmittance at 355 nm needed to be calculated (see SI Methods). The transmittance decreased with increasing  $t_{Ag}$  as expected (**Figure S1**). The only exception was the waveguide with  $t_{Ag}$  of 55 nm which had a slightly larger transmittance than the waveguide with  $t_{Ag}$  of 50 nm.

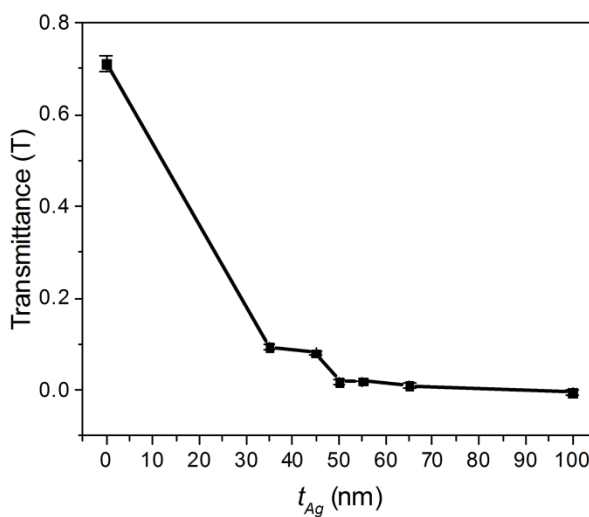


**Figure S1:** Transmittance at 355 nm as a function of  $t_{Ag}$ . Error bars represent  $\pm 1\sigma$  for 3 sample.

## S1.2 Reflectance Measurements

In order to calculate absorbance at 355 nm for the samples, the reflectance at 355 nm needed to be calculated (see SI Methods). All of the ISMI waveguides had similar reflectance values, indicating that reflectance remained relatively constant over the range of  $t_{Ag}$  in the ISMI waveguides (**Figure S2**).

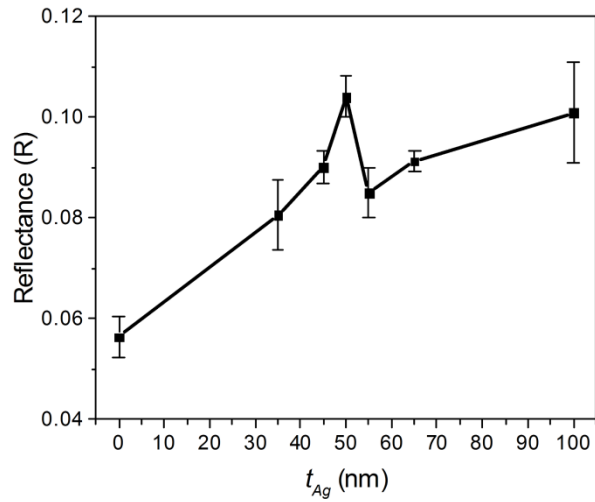


**Figure S2:** Reflectance at 355 nm as a function of  $t_{Ag}$ . Error bars represent  $\pm 1\sigma$  for 3 samples.

## S1.3 Absorbance Calculation

The absorbance for the waveguides at 355 nm was calculated by  $A_{355\text{nm}} = 1 - T_{355\text{nm}} - R_{355\text{nm}}$ . The absorbance increased significantly upon the addition of metal and increased slightly in the  $t_{Ag}$  range from 35 nm to 100 nm (**Figure S3**). This is expected because with thicker metal films the laser light can be reflected by the metal film more efficiently and thus more absorption can occur in the polymer layer.

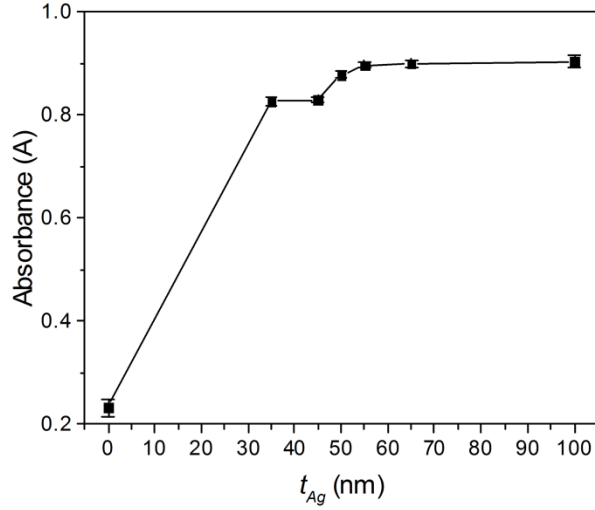


**Figure S3:** Absorbance at 355 nm as a function of  $t_{Ag}$ . Error bars represent  $\pm 1\sigma$  for 3 samples.

#### S1.4 ASE Slope Efficiency

The trend in ASE slope efficiency as a function of Ag metal film thickness (**Figure S4**) was virtually identical to the trends observed in the  $I_{max}$  and ASE threshold (Figure 4a and 4b). The slope efficiencies of the Ag metal containing waveguides from highest to lowest are as follows:  $4.2E11$ ,  $2.3E11$ ,  $2.9E10$ ,  $2.5E10$ ,  $1.3E10$ , and  $8.99E9 \frac{\text{counts} \times \text{cm}^2}{\text{W}}$  for ISMI waveguides with Ag metal film thicknesses of 45, 50, 55, 65, 100, and 35 nm, respectively.

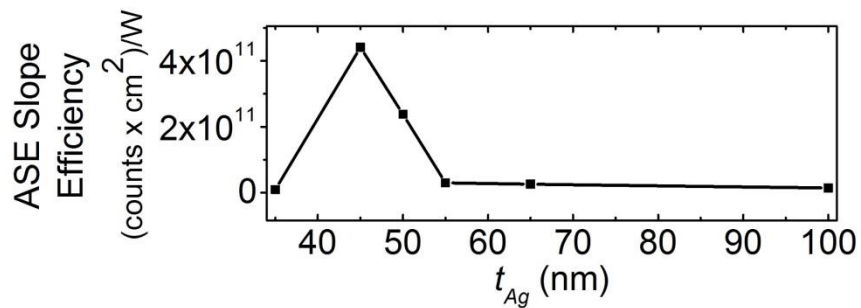


**Figure S4:** ASE slope efficiency of outcoupled edge emission from glass/PFO/Ag/glass ISMI waveguides with Ag metal film thickness of 35, 45, 50, 55, 65, and 100 nm under an excitation pump power density of  $1.8 \text{ mW}/\text{cm}^2$ .

### S1.5 Front-Face Peak Intensity Measurements

To detect leakage of SPPs in the direction orthogonal to the plane of the waveguide, a set of front-face emission spectra were collected (see SI Methods). Spectra were collected at an average pump power density of  $1.5 \text{ mW/cm}^2$  and  $0.14 \text{ mW/cm}^2$ , which are above and below the ASE threshold for all of the samples, respectively. Spectra collected at  $0.14 \text{ mW/cm}^2$  are shown in **Figure S5**. The peak intensities in the wavelength range 440 – 460 nm for below threshold were corrected for excitation power variation at 355 nm (due to the changes in Ag transmittance with varying thickness) and plotted as a function of  $t_{Ag}$  (**Figure S6**). The lack of a trend and the near 0 slope of the line indicate that there is no significant dependence of the front-face emission intensity with  $t_{Ag}$ . The above threshold plot exhibited similar slope (not shown).

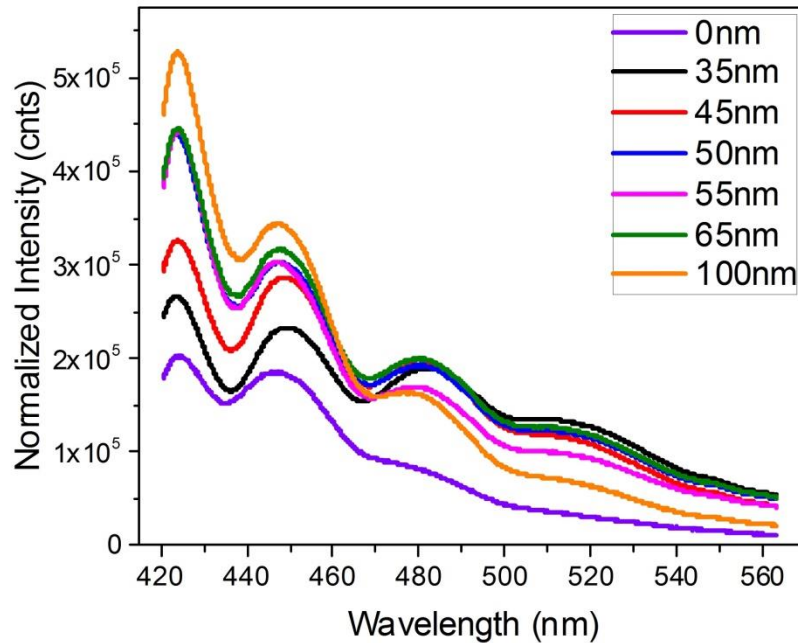


**Figure S5:** Front-face emission spectra for waveguides with metal film thicknesses of 0, 35, 45, 50, 55, 65, and 100 nm at an excitation pump power density of  $0.14 \text{ mW/cm}^2$ .

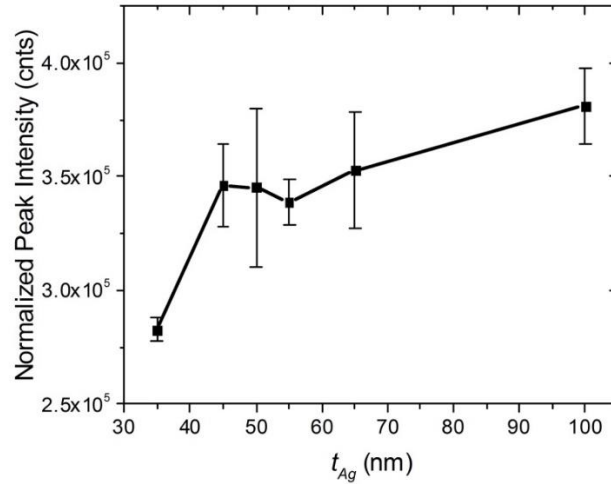


**Figure S6:** Peak intensities of front-face emission spectra from glass/PFO/Ag/glass ISMI waveguides with metal film thicknesses of 35, 45, 50, 55, 65, and 100 nm under an average excitation pump power density of  $0.14 \text{ mW/cm}^2$  as a function of Ag metal film thickness. The peak intensities were corrected for differences in excitation power at 355 nm due to changes in the transmission of Ag with film thickness at that wavelength. Error bars represent  $\pm 1\sigma$  for 3 samples.

### S1.6 Split TE and TM-polarized Peak Intensities

The split TE and TM-polarized peak intensities versus Ag film thickness, including the data for the ISI waveguide, is shown in **Figure S7**. A brief discussion of these results can be found in the discussion of Figure 6 in the main text.

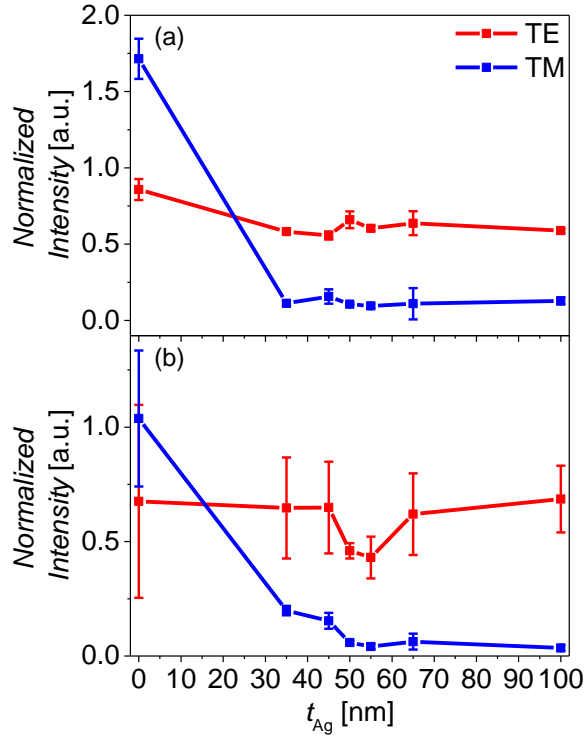


**Figure S7.** TE and TM peak intensities as a function of  $t_{Ag}$  for ISMI waveguides under an excitation pump power density of  $0.48 \text{ mW/cm}^2$  (a) and  $4.8 \text{ mW/cm}^2$  (b). Normalized by the unpolarized peak intensity and waveguide absorbance. Error bars represent  $\pm 1\sigma$  for 3 locations. This data is the same as plotted in Figure 6, however it also included ISI waveguide data (i.e.,  $t_{Ag}$  of 0 nm).

## S2. Supplementary Methods

### S2.1 Thermal Evaporation Conditions of Ag Films and Resulting Roughness

Shown in **Table S1** are the thermal evaporation conditions used for the Ag thin films in the ISMI samples and the resulting root-mean-squared (RMS) roughness of the Ag thin films measured by AFM. The deposition rate reading on the quartz crystal monitor was  $0.1 \text{ nm/s}$  for all of the Ag films. This is the lowest detection limit for the deposition rate reading using the thermal evaporation system. Even though the deposition rate reading was constant for all the samples, the average deposition rate, calculated by dividing the final Ag film thickness by the evaporation time, indicated that the deposition rates for the 35 nm- and 100 nm-thick Ag films were outliers. Since the average deposition rates were similar for most of the samples, the Ag

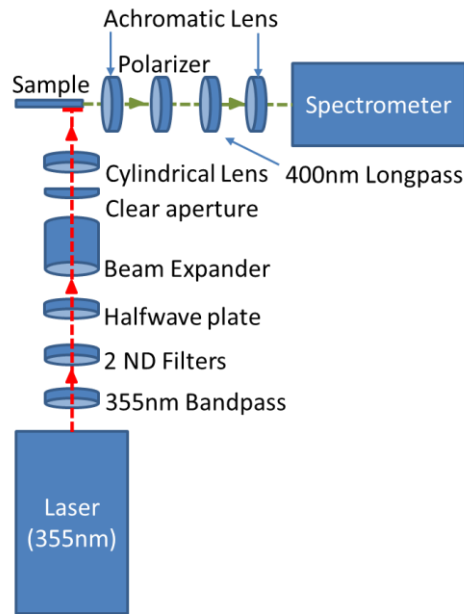
film roughness variations likely arose from other uncontrollable factors. The slight changes in pressure did not appear to affect the Ag film roughness.

ISMI Thermal Evaporation Conditions and Resulting Roughness					
Thickness (nm)	Pressure (mbar)	Deposition Rate Reading (nm/s)	Evaporation Time (min)	Average Deposition Rate (nm/s)	RMS Roughness (nm)
35	5.00E-06	0.1	41	0.014	2.30
45	6.00E-06	0.1	15	0.050	3.60
50	6.00E-06	0.1	17	0.049	2.93
55	6.00E-06	0.1	23	0.040	2.23
65	5.00E-06	0.1	22	0.049	2.44
100	5.00E-06	0.1	20	0.083	2.11

**Table S1:** Thermal evaporation conditions and roughness of Ag films used in ISMI waveguides.

## S2.2 Polarization-Dependent Set-Up Schematic

Shown in **Scheme S1** is the set-up for the polarization-dependent photoluminescence measurements.



**Scheme S1:** Schematic of polarization-dependent photoluminescence set-up.

### **S2.3 ASE Slope Efficiency**

Amplified spontaneous emission (ASE) slope efficiency was extracted from the plots of intensity at the peak emission wavelength ( $I_{max}$ ) versus power density by fitting two linear lines to the steady state and stimulated emission regions. The ASE slope efficiency is the slope of that line.

### **S2.4 Transmittance Measurements**

Measurements were done using an Ocean Optics OOIBase 32 with an integration time of 10 ms and 3000 averages. A dark and a reference were collected. The reference was a glass substrate and superstrate bonded with epoxy. 3 different locations on each sample were measured. These were the same materials used in fabricating the waveguides. The spectrometer used a tungsten-halogen bulb and functioned in the range 350 - 900 nm.

The spectra for each sample were averaged and plotted in Origin. The transmittance at 355 nm was recorded and plotted as a function of metal film thickness in the waveguides.

### **S2.5 Reflectance Measurements**

The laser set-up used to do reflectance measurements was similar to the front-face emission set-up (S2.5) with a few changes. Firstly, the dichroic mirror was replaced with a glass microscope slide in order to direct some of the 355 nm laser-light reflected from the sample into the spectrometer. Secondly, the 400 nm long pass filters were removed because the reflected intensity of the laser light was of interest. After focusing, spectra were collected at 3 different locations on each sample over the range 320 – 455 nm. A UV-mirror was placed at the sample location in order to collect the reference spectrum.

Using Origin all spectra were corrected for the ambient background and for variations in power. Then, the peak intensities at 355 nm for each sample were averaged and divided by the peak intensity at 355 nm from the reference spectrum in order to get the reflectance for each waveguide.

## **S2.6 Apparatus Used to Collect Front-Face Emission Spectra**

The apparatus used to collect front-face emission spectra of the ISI and ISMI waveguides was the same as the apparatus used to collect pump-power-dependent emission spectra (see paper) with a few additions. Firstly, a half-wave plate (Newport) set to  $45^\circ$  was placed before the Edmund Optics Galilean-type zoom beam expander 1-8X, to reduce polarization bias from the excitation source. Secondly, a dichroic mirror (Newport 400 nm short-pass filter) was placed at the sample location. The sample stage was moved backward. Therefore, the laser would pass through the dichroic mirror and hit the sample. The emission from the sample would be reflected off of the dichroic mirror and focused into the spectrometer with the existing optics. Because the sample was moved, the Edmund Optics Galilean-type zoom beam expander 1-8X, Output Clear Aperture 33 mm, and the cylindrical lens were all moved to get the best focused stripe on the sample.

The laser and spectrometer settings were the same as the settings used for the polarization-dependent emission spectra (see paper). It is worth to mention that a stripe was projected onto the spectrometer and a  $250\ \mu\text{m}$  vertical portion of the stripe was collected. Spectra were collected at three different locations on each sample from the middle of the sample. At each location, 2 spectra were collect at ND filter wheel settings of 0.24 OD and 1.2 OD, corresponding to an average power density of  $1.5\ \text{mW}/\text{cm}^2$  and  $0.14\ \text{mW}/\text{cm}^2$ , respectively.

These power densities are above and below the ASE threshold for all of the samples, respectively.

### **S2.7 Method of Front-Face Spectra Analysis**

Using Origin Pro 2015, all the spectra were first subtracted by the ambient background and corrected for variation in power. All the above threshold spectra were corrected to the same power and all the below threshold spectra were corrected to the same power. The peak intensity in the range 440 – 460 nm for the 3 spectra for each power density for each sample was averaged. The peak intensities were corrected for differences in absorbance by dividing the peak intensities by the absorbance at 355nm for each sample. The corrected peak intensities were plotted as a function of metal film thickness.